frontiers | Frontiers in Earth Science

TYPE Original Research
PUBLISHED 14 September 2022
DOI 10.3389/feart.2022.957337

OPEN ACCESS

EDITED BY
Fuhao Xiong,
Chengdu University of Technology, China

REVIEWED BY
Hu Huang,
Chengdu University of Technology, China
Qi Deng,
Chengdu Geological Survey Center, China

*CORRESPONDENCE
Tiannan Yang,
yangtn@cags.ac.cn

SPECIALTY SECTION
This article was submitted to Structural Geology and Tectonics, a section of the journal Frontiers in Earth Science

RECEIVED 31 May 2022
ACCEPTED 22 August 2022
PUBLISHED 14 September 2022

CITATION
Liang M, Yang T, Yan Z, Xue C, Xin D, Qi S, Dong M, Wang W, Shi P, Xiang K, Han X and Bao J (2022), Early Late Triassic retro-foreland basin in response to flat subduction of the Paleo-Tethyan oceanic plate, SE Tibet.
Front. Earth Sci. 10:957337.
doi: 10.3389/feart.2022.957337

Early Late Triassic retro-foreland basin in response to flat subduction of the Paleo-Tethyan oceanic plate, SE Tibet

Mingjuan Liang[1,2], Tiannan Yang[2]*, Zhen Yan[2], Chuandong Xue[3], Di Xin[2], Shaofeng Qi[1], Mengmeng Dong[2], Wei Wang[3], Pengliang Shi[4], Kun Xiang[5], Xue Han[6] and Jingkun Bao[3]

[1]Geological Museum of Guizhou, Guiyang, China, [2]Institute of Geology, Chinese Academy of Geological Sciences, Beijing, China, [3]Department of Earth-Sciences, Kunming University of Sciences and Technology, Kunming, China, [4]Beijing Jinyou Geological Exploration Co. Ltd., Beijing, China, [5]School of Resources and Environmental Engineering, Guizhou Institute of Technology, Guiyang, China, [6]Guizhou Geological Survey, Guiyang, China

Syn-subduction basins bear significant implications to understand tectonic evolution of any fossil subduction zone. The late Paleozoic to early Mesozoic (Paleo-Tethyan) tectonics of the eastern and southeastern Tibetan Plateau (i.e., the Sanjiang Orogenic Belt) is featured by ocean-continent subduction systems. A huge pile of volcanic-absent sedimentary succession developed in the middle segment of the Sanjiang orogenic belt, its age and tectonic nature remain unclear. Detailed geological mapping and zircon U-Pb dating results demonstrate that the early Late Triassic volcanic-absent succession comprises the nonmarine Maichuqing Formation in the lower part and the shallow marine Sanhedong Formation in the upper part. The Maichuqing Formation consists of coarse to fine-grained sandstone, siltstone and mudstone with abundant basal erosional surfaces, trough and planar cross-beddings, ripples, mudcracks, and plant fragments. The Sanhedong Formation comprises predominantly bioclastic limestones interlayered with marl, calcareous-muddy siltstone, and calcareous sandstone with abundant bivalve fossils. Syn-sedimentation deformation structures, such as slump folds and associated normal faults are common, suggesting intense tectonism during deposition. Synthesizing sedimentary data, paleocurrent and provenance results, combined with other available data, demonstrate that the volcanic-absent succession deposited within a retro-foreland basin along the rear part of the Permian-Triassic Jomda-Weixi-Yunxian arc in response to flat-subduction of the Paleo-Tethyan Ocean during the early Late Triassic time.

KEYWORDS

sedimentary environment, early Late Triassic, retro-foreland basin, flat subduction, SE Tibet

1 Introduction

Subduction of oceanic plate between two continents commonly ended by collision of these two continents. Sedimentary basins of different types may develop during each stage of the process from subduction to collision, whereas the natures of these basins well reflect tectonic regimes of each individual stage of the related orogenic belt (Allen and Allen, 2005; Hu et al., 2016). For example, retro (arc)-foreland basin commonly develops at leading edge of the folded part of an arc as a flexural response to crustal shortening in a compressional setting (Jordan, 1995). As such, identification of a retro foreland basin (Decelles and Giles, 1996; García-Castellanos, 2002; Decelles et al., 2011), combined with geochemistry and structure of arc-volcanic rocks, may much better constrain subduction dynamics of the related subduction zone than by evidence from any single principle.

Tectonic facies analysis (e.g., Burchfiel and Chen, 2012; Yang et al., 2012, 2014; Xin et al., 2018) shows that the late Paleozoic to Early Mesozoic (Paleo-Tethyan) tectonics of the northern, eastern, and southeastern Tibetan Plateau (Figure 1A) are featured by subduction of oceanic plates and subsequent continental collisions. At present time, less attention has been paid to any subduction- or collision-related sedimentary basin (Burchfiel and Chen, 2012). As the result, the Paleo-Tethyan tectonics of these regions is still hotly debated, on which, our understanding was derived mainly from geochemical and geochronological studies of igneous rocks (e.g., Wang et al., 2011, 2014).

Geological mapping results with scale 1/200,000 (Edit Committee of the Sanjiang Geological Map, 1986) have revealed an Upper Triassic volcanic-absent succession in the eastern Tibetan Plateau, which was termed as the transitional unit by Burchfiel and Chen (2012). This unit gradually changes northwestward into the Late Triassic Yushu-Yidun arc belt (Yang et al., 2012) and southward into the Late Triassic Yunxian arc belt (Figure 1B). Given most Triassic rocks in the eastern and southeastern Tibetan Plateau are volcanic-bearing, the forming of such a volcanic-absent sedimentary unit is still a puzzle.

In this study, we try to document the stratigraphic architecture of the transitional unit and discuss its sedimentary environments according to the sedimentary textures and syn-sedimentation deformation structures. Its depositional time was determined based on zircon U-Pb age data. These new data and other available data were used to discuss the forming process and tectonic nature of the transitional unit.

2 Tectonic background

The Paleo-Tethyan tectonics of the eastern and southeastern Tibetan Plateau (i.e., the Sanjiang orogenic belt; Figures 1A,B) is featured by two ocean-continent subduction systems. The major ocean-continent subduction system consists of the huge early Permian to late Triassic Jomda-Weixi-Yunxian arc (Yang et al., 2014) to the northeast or to the east and the Longmu co-Shuanghu-Changning-Menglian suture (Mo et al., 2001; Li et al., 2006) to the south or to the west. This system is commonly interpreted as the results of the northeastward or eastward subduction of the Paleo-Tethyan Ocean beneath the Eastern Qiangtang Continent (northern segment) and the Lanping-Simao Continent (southern segment; Xin et al., 2018). Another ocean-continent subduction system comprises the Upper Triassic Yushu-Yidun arc to the south and the western Jinshajiang–Garzê–Litang suture to the north. This system was formed by southward subduction of the Garzê-Litang Ocean beneath the Qiantang Continent during the middle to late Triassic (Yang et al., 2012).

The Jomda–Weixi–Yunxian arc consists of three segments with different magmatism history (Xin et al., 2018). The northern segment contains a long-lasting magmatic evolution from the early Permian to middle Triassic (Yang et al., 2011). The subduction-related magmatism of the middle segment is short-lived and exhibits an early to middle Triassic magmatic flare-up (Xin et al., 2018). The southern segment contains a long-lasting magmatic evolution as well, consisting of several pulses of magmatism from middle Permian to late Triassic (Yang et al., 2014). The Triassic volcanic-absent transitional unit is spatially coinciding with the middle segment of the Jomda–Weixi–Yunxian arc. Its northern and southern boundaries with the Late Triassic Yushu–Yidun arc volcanoclastic rocks and the Late Triassic volcanoclastic rocks of the southern segment of the Jomda–Weixi–Yunxian arc, respectively, are both gradual. The eastern boundary of the transitional unit is not very clear, where Late Triassic sedimentary rocks are conformable with the underlain shallow marine platform sedimentary rocks of the Yangtze Block (Burchfiel and Chen, 2012). On contrary, its western boundary is an unconformity, along which the volcanic-absent rocks overlie the middle segment of the Jomda–Weixi–Yunxian arc, where the subduction-related volcanoclastic rocks are tightly folded (Yang et al., 2012; Liang et al., 2015; Tang et al., 2016; Xin et al., 2018). This spatiotemporal relationship between these tectonic units (Figure 1B) makes it hard to understand tectonic nature of the basin represented by volcanic-absent sedimentary rocks of the transitional unit (Burchfiel and Chen, 2012). Widespread Mesozoic and Cenozoic basins, such as the Cretaceous Lanping basin (Liang, 2017 and references therein) and the Eocene Jianchuan basin (Liao et al., 2020) as well as the crustal deformation induced by the India–Eurasia collision (Yang et al., 2021; Liang et al., 2022) worse the situation.

This paper focuses on the tectonic nature of the transitional unit. On basis of geological mapping with scale 1/50,000 in the Lanping and Madeng areas (Figure 2A; Liang et al., 2022), we conducted detail sedimentary studies along the Misha–Xiangtu profile and in the open mining pits of the supergiant Jinding Zn–Pb deposit (Song et al., 2020). The locations of the study areas are marked in Figure 2A.

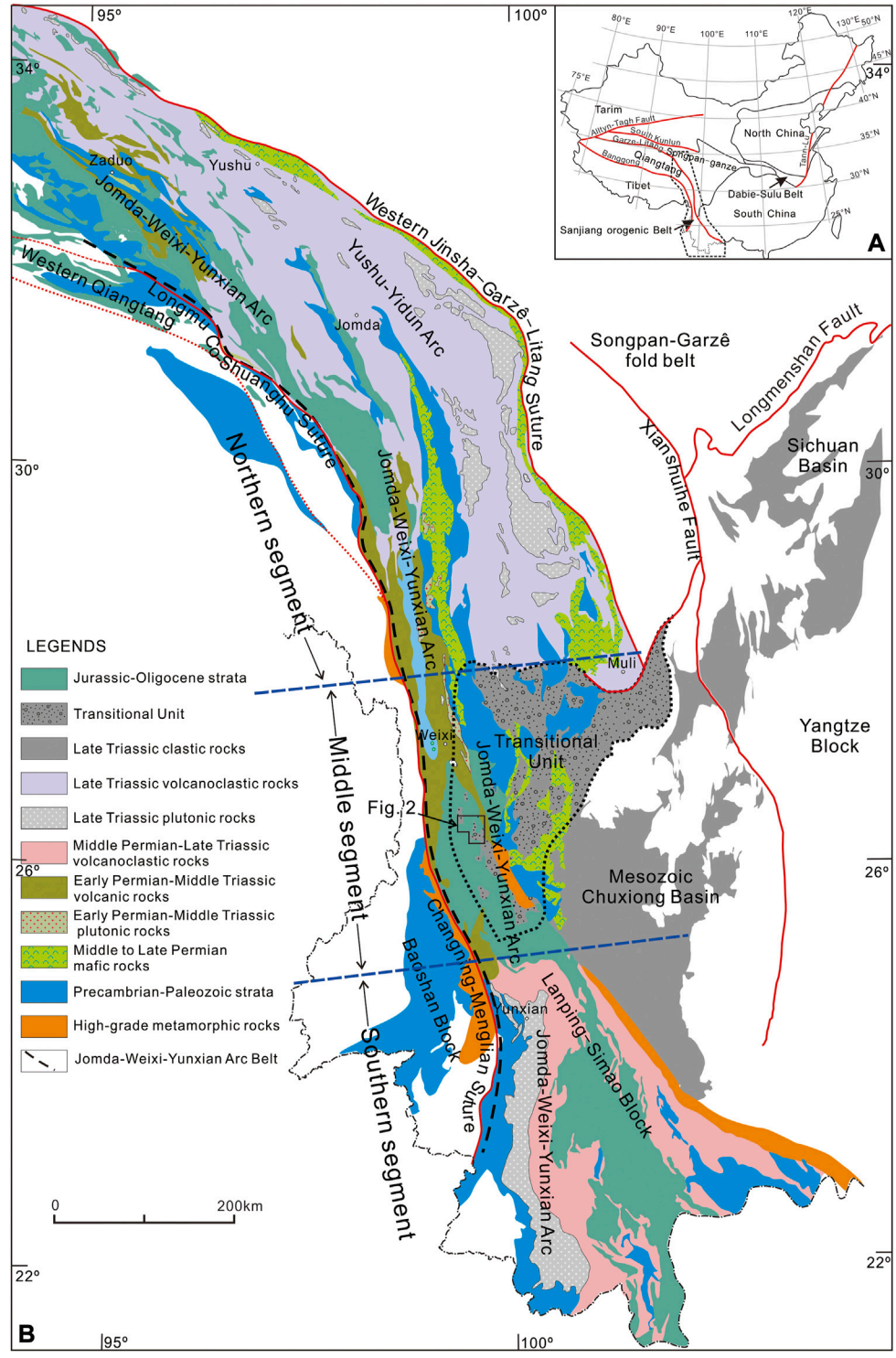

FIGURE 1
(A) Tectonic framework of China mainland showing the location of the Sanjiang orogenic belt. **(B)** Simplified geological map of the Sanjiang orogenic belt showing the tectonic framework and the locations of the Transitional Unit (thick dash-line) and the study area (the solid polygon) (modified after ECSGM, 1986; Burchfiel and Chen, 2012; Yang et al., 2014, 2021). The two blue dashed lines are the approximate boundaries separating the northern, middle, and southern segments of the Jomda–Weixi–Yunxian arc belt, respectively.

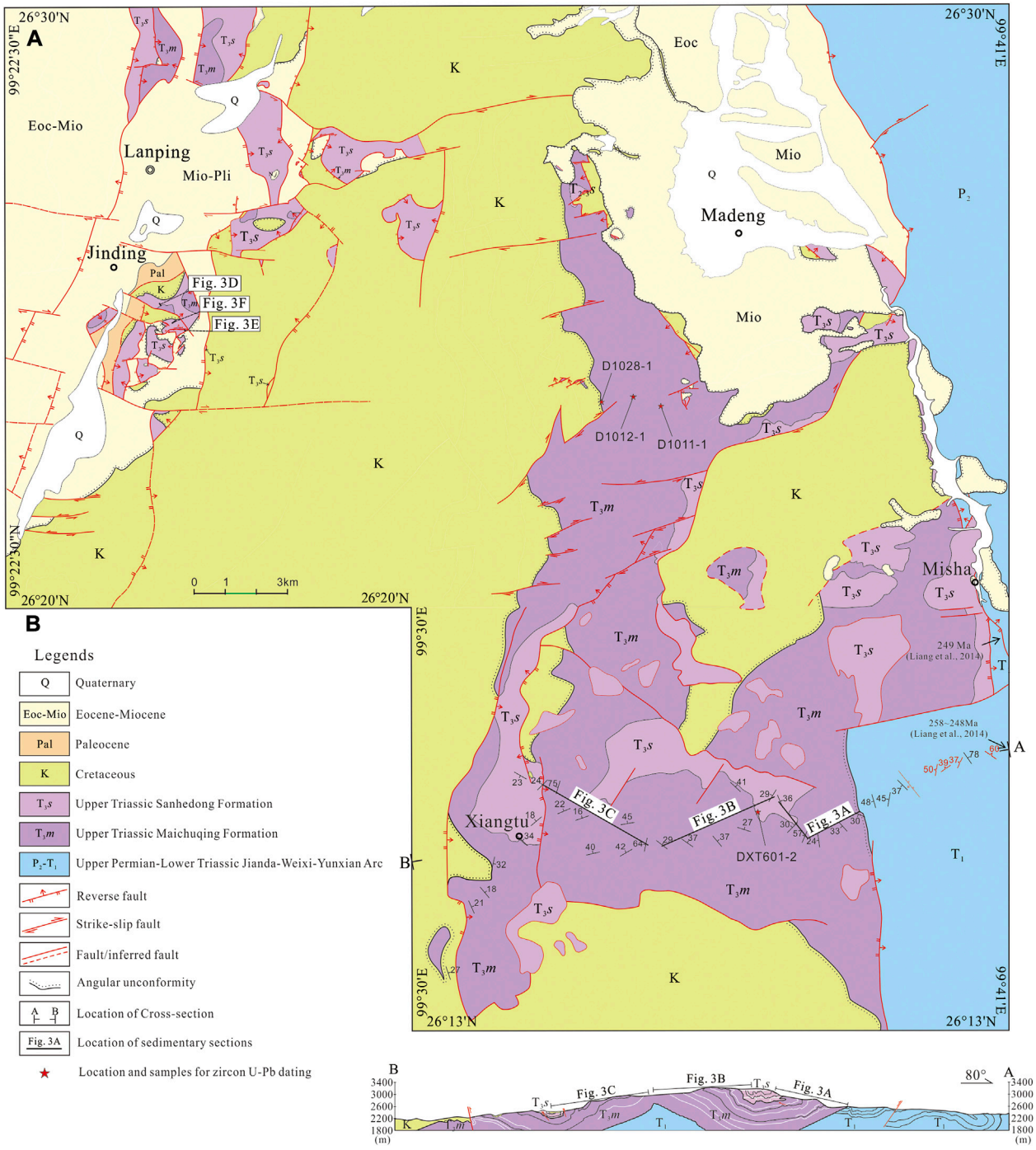

FIGURE 2
(A) Geologic map of Jinding–Madeng–Misha–Xiangtu area in the northwest Yunnan Province, China. Its location was marked in Figure 1B. **(B)** Cross-section showing the structures and contact relationships between the Upper Triassic and underlain strata along the Misha to Xiangtu profile.

3 Sedimentary facies and depositional environments

The Late Triassic sedimentary rocks of the Lanping and Madeng areas are exposed as numerous isolated patches of irregular outlines setting in a groundmass of Cretaceous red-beds. These Triassic sedimentary rocks were initially defined as the Maichuqing Formation (T_3m) in the lower part and the Sanhedong Formation (T_3s) in the upper part based on their rock assemblages and associated fossils by YBGMR (1974). Both

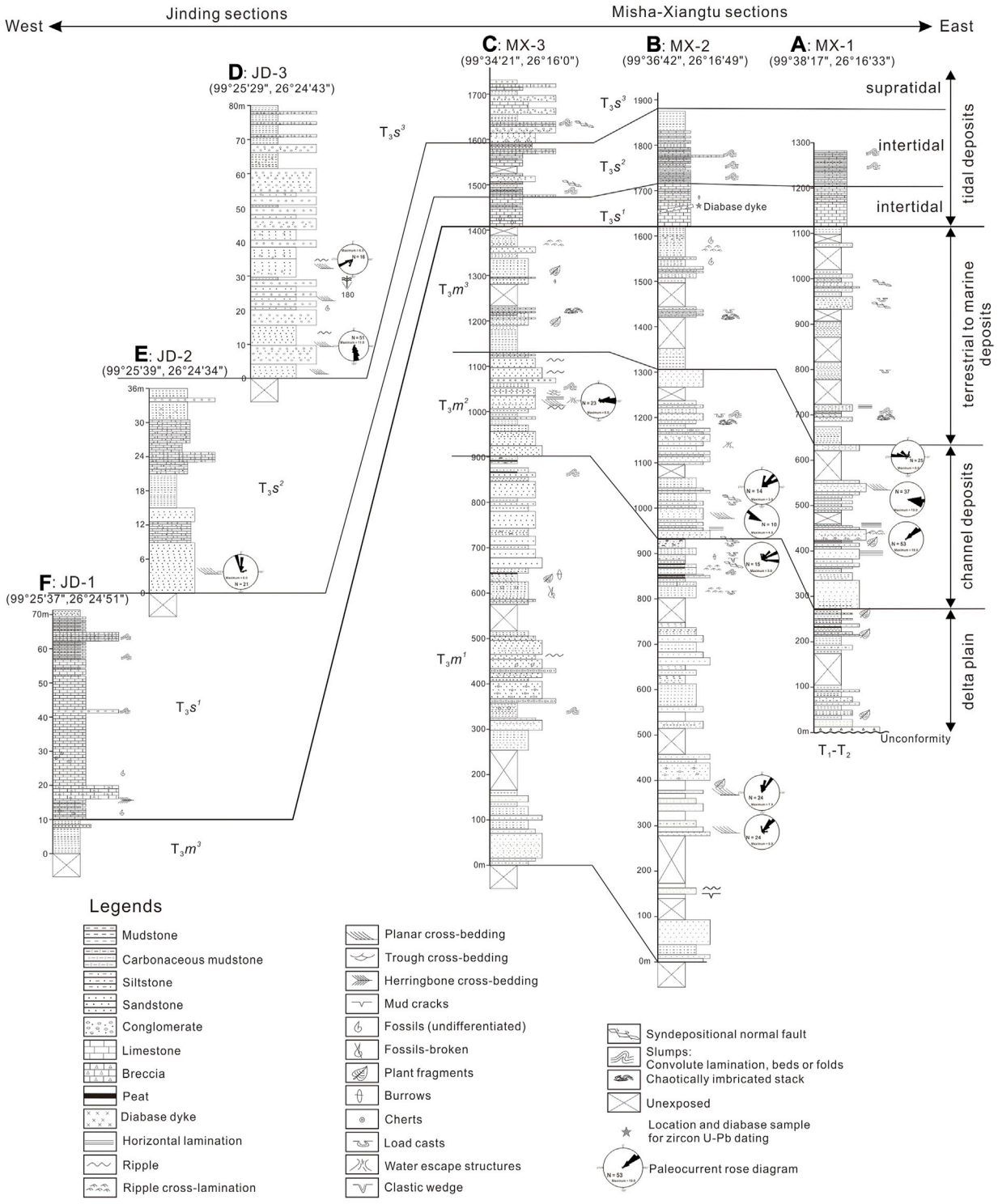

FIGURE 3
Measured sedimentary logs of the Maichuqing and Sanhedong formations. See Figure 2A for the locations of each section. From east to west, the three sections **(A–C)** along the Misha–Xiantu profile show successive variation in sedimentary features of the Maichuqing and Sanhedong formations, whereas the Jinding sections **(D–F)** show the lower, middle and upper part of the Sanhedong Formation. Note that the paleocurrent data of the Jinding section are not used to discuss because of the uncertainty in rotation of the related small fragments (see Figure 2A).

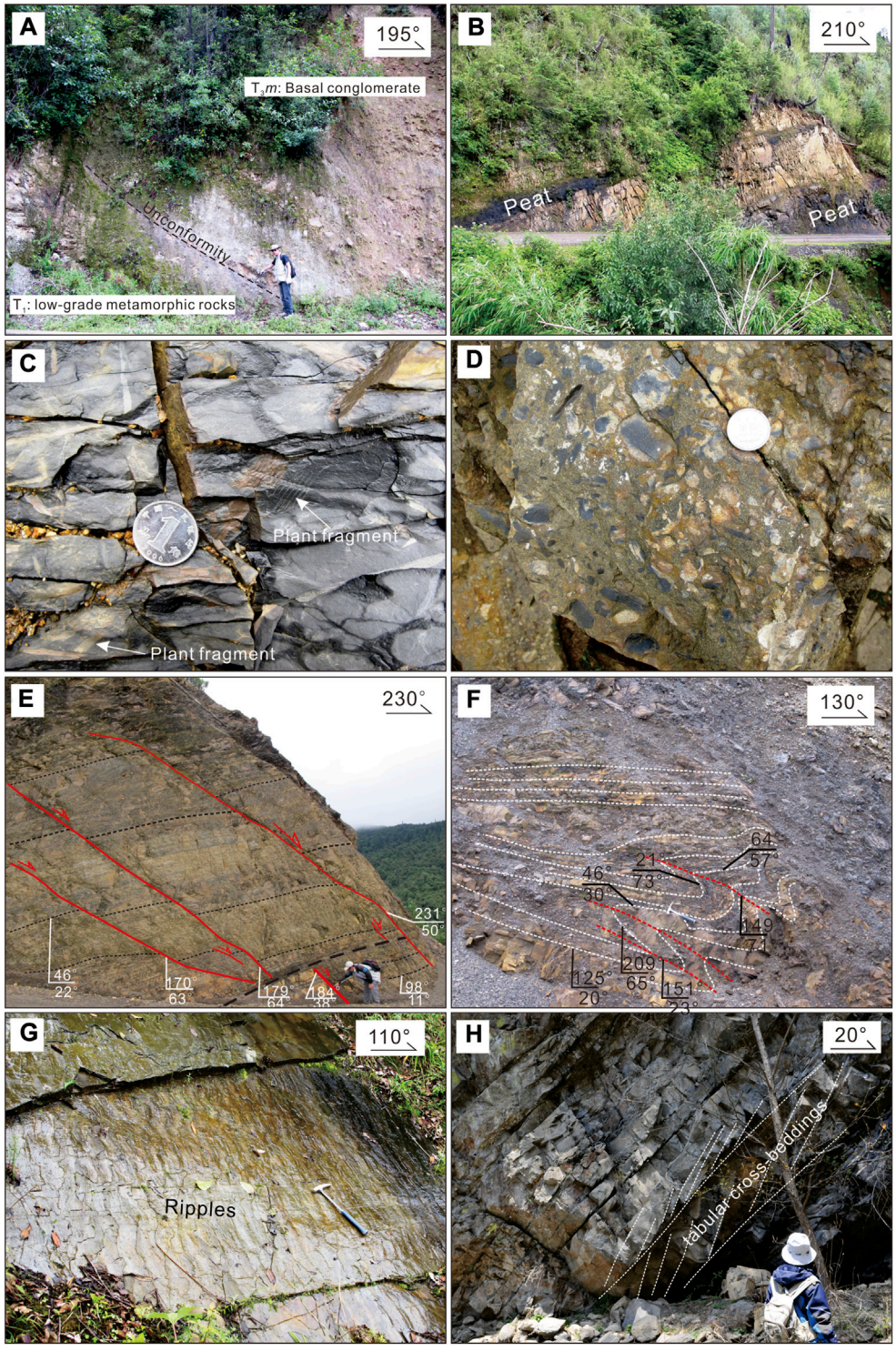

FIGURE 4
Field photographs showing typical sedimentary features of the Maichuqing Formation. **(A)** The Maichuqing Formation nonconformably overlies the early Triassic low-grade metamorphic rocks (GPS: 99.38′17″, 26.16′33″); **(B)** Peats in the high level of the lower segment of the Maichuqing Formation; **(C)** Plant fragments in siltstone; **(D)** Conglomerate; **(E)** and **(F)** Syn-sedimentation faults and folds in siltstone and mudstone; **(G)** Ripples in siltstone; **(H)** Planar cross-beddings of sandstone.

formations are well exposed in the Madeng–Misha area and the open pits of the supergiant Jinding Pb–Zn deposit. In the Misha–Xiangtu profile (Figure 2B), they folded and exhibited two open synclines and an open anticline. As such, the repeating of any stratigraphic units (see the sections MX-1 to 3 of Figure 3) shows the changes in thickness, sedimentary textures, and rock assemblage of the related units.

3.1 The Maichuqing formation

The ca. 1,100~1,650-m-thick Maichuqing Formation noncomfortably overlies the volcanoclastic rocks of the Jomda–Weixi–Yunxian arc (Figure 2A). This formation contains three segments according to the rock assemblages and associated sedimentary structures. In addition, the thickness, rock assemblage, and sedimentary texture of these three segments are variable from east to west, showing a westward thickening sequence (Figures 3A–C).

3.1.1 Lower segment

The lower part of the Maichuqing Formation consists of conglomerate, sandstone, siltstone, mudstone and lenticular peats. In the MX-1 section, it is ca. 270 m thick and nonconformably overlies the volcanoclastic rocks of the Jomda–Weixi–Yunxian arc (Figure 3A). Ca. 12-m-thick conglomerates exist at the bottom. They are matrix-to clast-supported and dominated by slate, phyllite, mudstone and sandstone clasts. These clasts originated from the underlain rocks of the Jomda–Weixi–Yunxian arc (Figure 4A) based on their same lithology. The conglomerate graded upward into an assemblage of siltstone, mudstone and sandstone with coalbeds or peats on the topmost (Figure 4B). Both sandstone and siltstone contain abundant plant fragments (Figure 4C).

To the west, the lower part of the Maichuqing Formation has a thickness of >900 m, where the underlain rocks and associated unconformity are not exposed (Figures 3B,C). In the MX-2 section, the equivalent consists of coarse-grain sandstone, siltstone, and mudstone; mud clasts common occur within siltstone and sandstone. Mud-cracks and ripple cross-laminations as well as normal grading and ripples are common, whereas slumped folds and syn-sedimentary normal faults were widely developed (Figures 4E,F).

To the west further in the MX-3 section, a suite of conglomerate (Figure 4D), pebbly coarse-grained sandstone, sandstone and siltstone with a thickness of ca. 150 m develops in the middle part of the lower segment. Other rocks both below and above the suite are the assemblages of sandstone and mudstone. Thinner siltstone, mudstone, and lenticular sandstone with several interbedded peats occur in the high level of the lower segment. These rocks are characterized by abundant burrows, plant fragments, ripple laminations. These characters demonstrate that they should deposit in a swamp environment. In addition, mud-cracks also occur in the mudstones, indicating that these fine-grained sediments experienced subaerial exposure. Conspicuous irregular basal erosional surface and imbricated clasts are easily observed in the outcrops of the conglomerate-bearing suite, indicating a channel environment (Miall, 1985). These observations demonstrate that the lower portion of the Maichuqing Formation deposited in channel, levee, and swamp environments of a delta plain (Miall, 1985).

3.1.2 Middle segment

The middle segment of the Maichuqing Formation consists of dark-gray sandstone, dark siltstone, and dark-gray calcareous mudstone with minor lenticular pebbly sandstone, showing a decreasing total thickness from 350 m in the east to 200 m in the west. Sandstones are massive, thin-to medium-bedded, and fine-to medium-grained, showing normal grading with distinct erosional base. Reverse grading also occurs locally. Siltstone is thinner and has parallel laminations, showing rhythmic sequence with mudstone. Conglomerate lenses occur in the high level with a thickness of <5 m, which extends laterally into the sandstone with distinct basal erosion surface. They are characterized by imbricated clasts comprising carbonaceous mudstone and mica-bearing medium-grained sandstone. Symmetrical ripples and trough cross-beddings widely occur in the thick, fine-grained sandstone (Figure 4G). Planar and trough cross-beddings are common within the sandstones in the upper level (Figure 4H); load casts are also observed locally. Slump folds occur near top of this part. We interpreted these sedimentary rocks as channel deposits of the delta plain (Miall, 1985).

3.1.3 Upper segment

The upper segment of the Maichuqing Formation has a variable thickness of ca. 260–450 m, which is dominated by interlayers of grey mudstone and siltstone. Lenticular sandstones and minor peats also occur locally in different sections. Abundant plant leaves fossils exist within the siltstone and mudstone at the lower level, and some lamellibranch fossils, including *Burmesia lirata* Healey, *Cuspidaria* sp., *Prolaria sollasii* Healey, and *Nuculanna* cf. *perlonga* (Mansuy), also exist at the upper level (YBGMR, 1974). Spatially, abundance and thickness of siltstone and sandstone increase vertically and to the west. Lenticular, ripple and parallel laminations are common in the sandstone and siltstone, and slump folds and normal faults also occur within mudstone. These characters demonstrate that the upper part of the Machuqing Formation deposited in a transitional environment from terrestrial to marine setting (Reading, 1996).

3.2 The Sanhedong Formation

The exposed thickness of the Sanhedong Formation is >300 m (Figure 3). This formation conformably overlies the

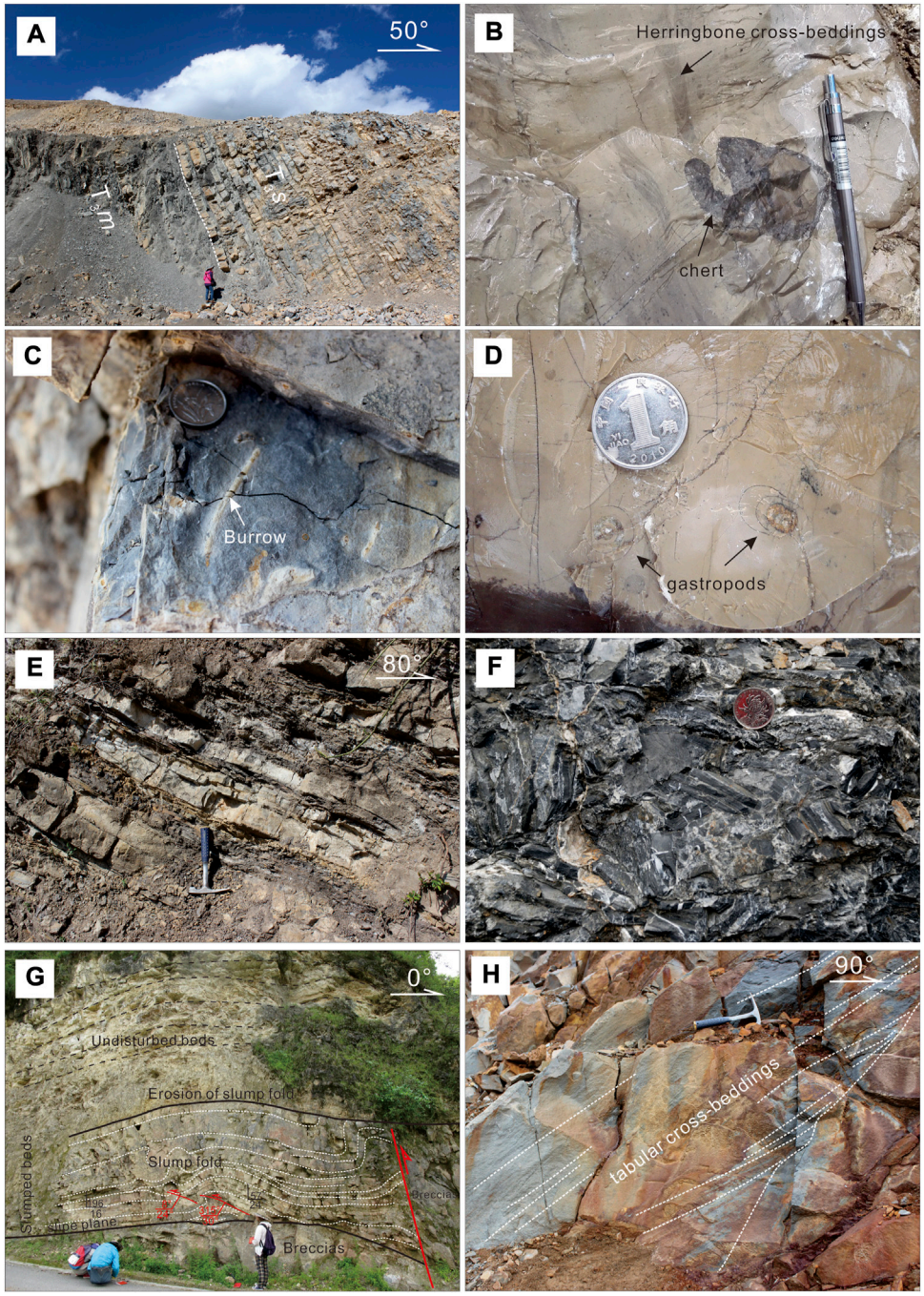

FIGURE 5
Field photographs showing the typical sedimentary features of the Sanhedong Formation. **(A)** Conformable contact between the Sanhedong Formation and the Maichuqing Formation (GPS: 99°25′37″, 26°24′51″); **(B)** Herringbone cross-beddings and chert nodules within micrite; **(C)** Burrows within thick limestone; **(D)** Gastropod fossil in micrite; **(E)** Thinly bedded micrite and marl with minor calcareous mudstone; **(F)** Brecciated limestone; **(G)** Slumped folds of thinner calcareous mudstone and micrite and associated brecciated limestone; **(H)** Tabular cross-beddings of sandstones.

Maichuqing Formation (Figure 5A) and can be subdivided into three segments based on its rock assemblages. *Halobia pluriradiata* Reed and *H.* cf. *yunnanensis* Reed in the upper part and some ammonoid, brachiopoda, lamellibranchiate in the lower part of this formation (YBGMR, 1974) indicate a shallow marine environment of depositional setting.

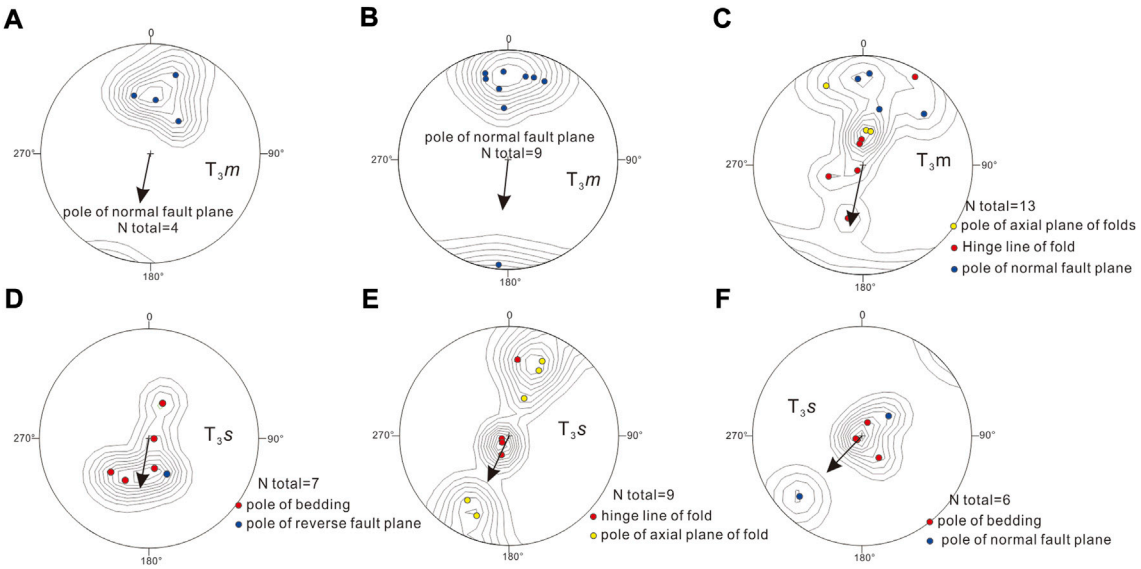

FIGURE 6
Equal angle stereonet projections of planes of syn-sedimentation normal fault and axial planes of slump folds. See text for detailed discussions. "N" means total number of measured altitudes of related structural elements.

The lower segment of the Sanhedong Formation consists of chert nodules-bearing micrite (Figure 5B) and bioclastic limestone with interbedded calcareous mudstone. It was crosscut by 220.0 ± 7.7 Ma diabase sheet (see the following) in the outcrops. The micrite and bioclastic limestone are thinly bedded with abundant euhedral pyrites. Locally, some brecciated limestones are associated with slump folded limestone. Burrows occasionally exist in thick limestone and thinner mudstone (Figure 5C). Bivalves, gastropods (Figure 5D), and crinoids within limestone have a good shape. Herringbone cross-beddings (Figure 5B) and ripples can be easily observed in the outcrops of micrite. These observations demonstrate they deposited in an intertidal environment (Reading, 1996).

The middle segment comprises thinly bedded micrite and marl with minor calcareous mudstone and siltstone interlayers. The thickness of any single bed of micrite varies from 10 cm in the lower part to 3 cm in the upper part in association with an upward increasing of the abundance of mudstone and siltstone (Figure 5E). Micrites are similar to those in the lower segment, both have been heterogeneously brecciated. Laterally, abundance and thickness of brecciated limestone increases dramatically from Xiangtu in the east to Jinding in the west (Figure 2). The brecciated limestone is characterized by numerous angular fragments of micrite with a variable length of 1.5–10 cm (Figure 5F). These fragments are cemented by calcic sands or muds. Alternatively, slumped folds developed in the interlayers of thinner calcareous mudstone (Figure 5G). Irregular bituminous veins occur within the micrite. Conspicuous basal erosion surfaces are common at the bottom of the micrite and brecciated limestone. In addition, wavy and flaser beddings (Figure 5E) exist locally in the marl. Planar cross-beddings occur in the lower level and lenticular conglomerates occur in the high level. These characters demonstrate that these rock assemblages belong to channel deposits of the intertidal setting (Reading, 1996).

The upper segment of the Sanhedong Formation was mainly exposed in the Xiangtu (Figure 3C) and Jinding lead-zinc mining areas (Figures 3D–F). It consists of calcareous conglomerate, coarse-grained calcareous sandstone, calcarenite, brecciated limestone and minor micrite and mudstone. The conglomerates consist of angular-subrounded limestone pebbles with distinct large-scale-scoured basal surface. Size of clasts and thickness of the conglomerates increase upward. The sandstone is thick and made of subrounded quartz, chert fragments, and minor feldspar. Slumped folds and associated normal faults are common in the Xiangtu area. Ripples, wave and flaser laminations are common in calcarenite, while mudcracks occur in mudstone. These observations indicate that these rocks deposited in a supratidal environment and experienced subaerial exposure (Reading, 1996), where the sandstones with tabular cross-beddings (Figure 5H) and associated lenticular conglomerates represent channel deposition.

4 Paleocurrent data

We measured 522 planar cross-beddings, ripple laminations, ripples, and imbricated clasts at suitable outcrops so as to provide information for source location and basin paleogeography of the

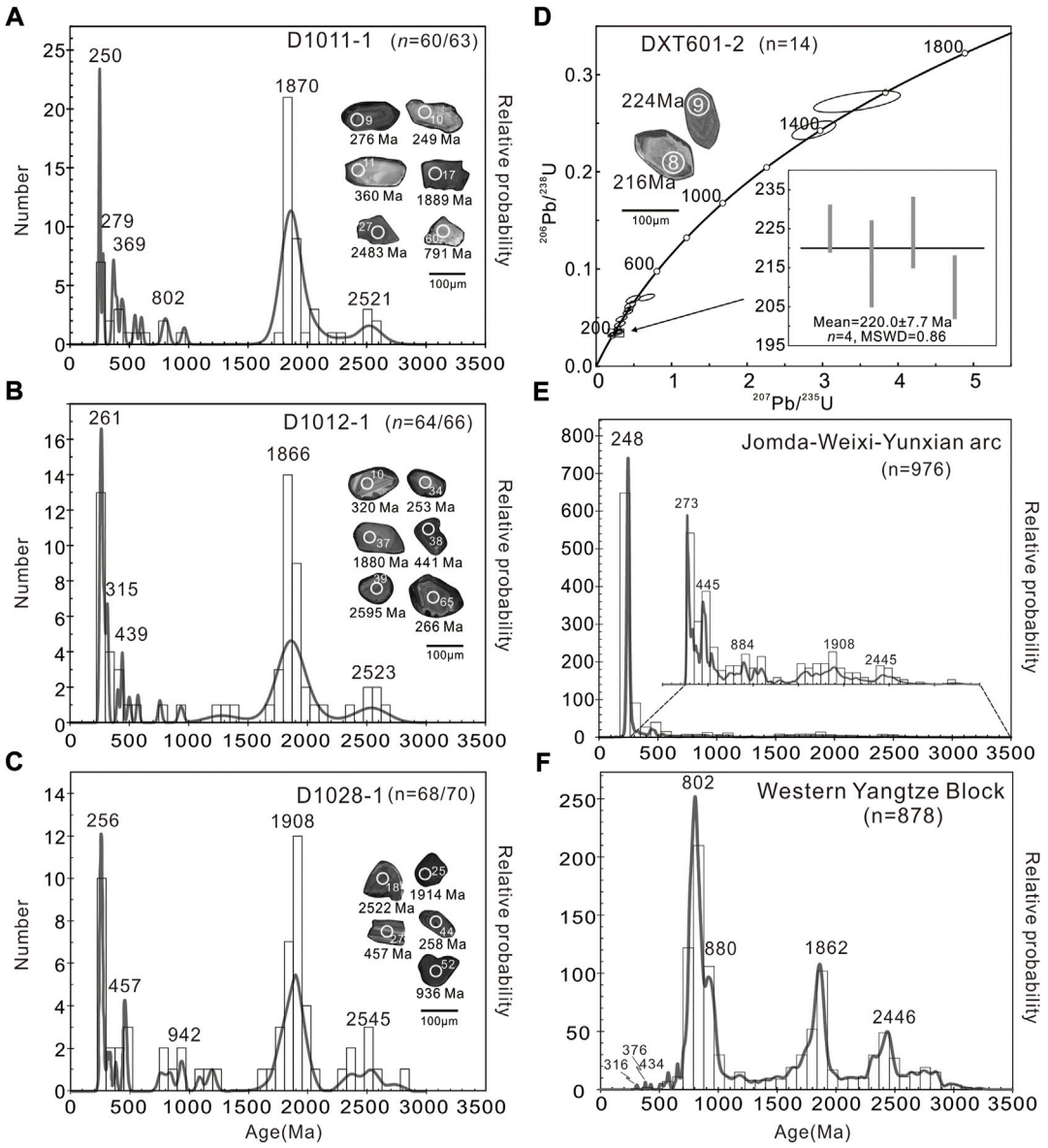

FIGURE 7
(A–C) Probability histograms of detrital zircon U-Pb ages of sandstone samples of the Maichuqing Formation. **(D)** Zircon U-Pb concordia diagram for the diabase dyke that intrudes the Sanhedong Formation. Relative probability of zircon U-Pb ages for igneous rocks of the middle Jomda–Weixi–Yuanxian arc **(E)** and for the western Yangtze Block **(F)** data sources: Sun et al., 2009 and Wang et al., 2012).

Maichuqing and Sanhedong formations (Figure 3). All data were corrected for local dip but not for possible later rotation because of lack of any regional rotation data to use as reference. However, geological mapping results demonstrate that 90 of the 522 measurements were located in some small blocks where available structural analysis results (Liang et al., 2022) show that these small blocks experienced heterogeneously rotation by thrust-and-tear fault associations. The remnant 432 measurements were conducted in the Misha–Xiangtu profile, along which the Late Triassic sedimentary rocks expose as a relatively complete block. Their results display that lower part of the Maichuqing Formation has a paleocurrent azimuth from 35° to 65°, but the lower and high levels of the middle part have two paleocurrent azimuths of 55°–100° and 275°–310°, respectively.

Syn-sedimentation deformation refers to sedimentary instabilities when the sediments in a slope were not solidified (Allen, 1982; Postma, 1983; Steen and Andresen, 1997; Moretti and Sabato, 2007). Abundant syn-sedimentation deformation structures in the Late Triassic rocks of the Misha-Xiangtu profile can also help us to infer basin paleogeography (Ortner,

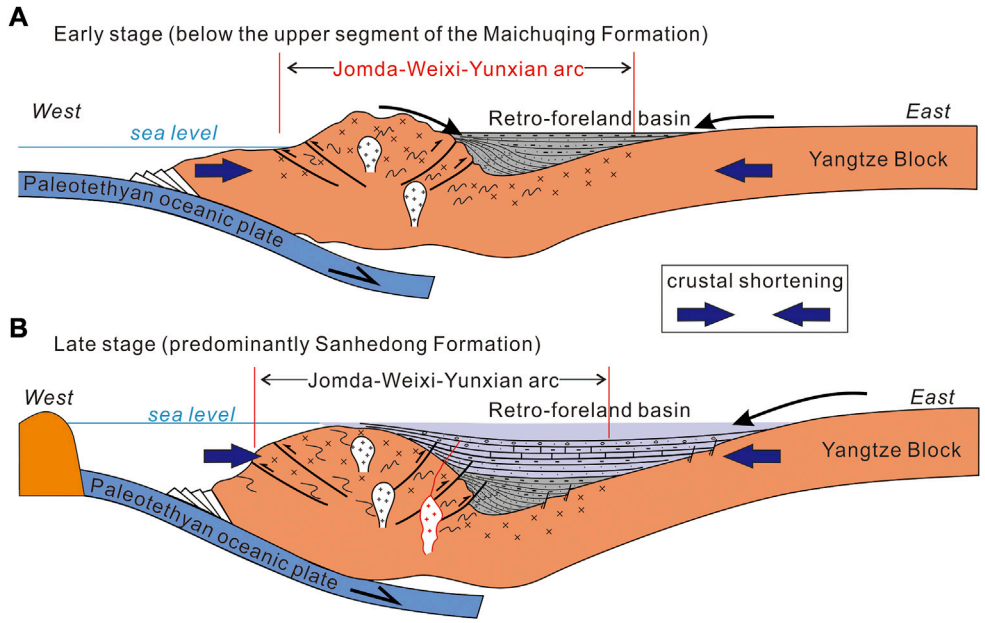

FIGURE 8
Cartoons show the development of the early Late Triassic retro-foreland basin, SE Tibet. See text for detail discussion.

2007; Lee and Phillips, 2008; Alsop and Marco, 2011; Lunina et al., 2012). Normal fault in high levels of the lower part of the Maichuqing Formation indicate 190°~200°-directed sliding of sediments (Figures 6A,B), Geometry of the recumbent slump folds supports this suggestion (Figure 6C). Intraformational reverse faults and overturned fold in the middle part of the Sanhedong Formation suggests 170°~190°-directed movement along the slipping plane (Figure 6D). Intraformational reverse faults and associated overturned folds in the middle part of the Sanhedong Formation suggest SSW-directed movement along the slipping plane (Figures 6D–F).

5 Zircon U-Pb ages of sandstones and diabase

In order to determine the timing of sedimentation and to reveal the provenance of the Triassic sedimentary rocks, three sandstone samples (D1011-1, D1012-1, and D1028-1) were collected from the middle portion of the Maichuqing Formation for detrital zircon U-Pb dating and one diabase dyke sample (DXT601-2) was collected to separate zircons for U–Pb dating, which intruded into the Sanhedong Formation. The locations of these samples are marked on Figure 2.

Zircons were separated using standard crushing, heavy liquid, and magnetic techniques. Exception for sample DXT601-2 that only 40 zircon grains were obtained, 150 to 200 zircon grains were hand-picked from the >25 μm non-magnetic fraction of each sandstone sample. Zircon grains were then mounted and cast in epoxy resin discs for photographing under reflected and transmitted light, obtaining cathodoluminescence (CL) images, and performing laser ablation LA-ICP-MS U-Pb dating. The U-Pb analyses of zircon were undertaken at the University of Science and Technology of China in Hefei, China, using an ArF excimer laser system (GeoLas Pro, 193 nm wavelength) and a quadrupole ICP-MS (PerkinElmer Elan DRCII). Analyses involved an ablation pulse rate of 10 Hz, beam energy of 10 J/cm^2, and a spot diameter of 32 μm. Procedures were described by Yuan et al. (2004). Standard zircon 91,500 (Wiedenbeck et al., 1995) was used for mass discrimination and elemental fractionation corrections, and U-Pb ratios were determined using the Excel program LaDating@Zrn. Common Pb was corrected by ComPb corr#3-18 (Anderson, 2002). Final statistics and age calculations were processed using Isoplot/EX ver. 4.15. We used $^{206}Pb/^{238}U$ and $^{207}Pb/^{206}Pb$ ages for zircons younger and older than 1.0 Ga, respectively (Griffin et al., 2004). Grains with >10% age discordance were discarded. Detailed procedures of zircon age determinations and trace-element analyses are followed Liu et al. (2007). Zircon U-Pb results are shown in Supplementary Table 1 with 1σ uncertainties.

5.1 Sample D1011-1

Sixty-three zircon grains with well-developed growth zonings yielded sixty concordant U–Pb ages of 2604–246 Ma. These spots can be grouped into two age populations of 246-963 Ma and

1,794–2,604 with a main peak at ca. 250 Ma, a secondary peak at ca. 1,870 Ma, and several minor peaks at ca. 369, ca. 802 and ca. 2,521 Ma (Figure 7A). They have a variable U content of 8–401 ppm and Th/U ratio of 0.06–4.09.

5.2 Sample D1012-1

Sixty-six zircon grains with well-developed growth zonings were analyzed and 64 of which yielded a concordant U–Pb age, ranging from 2,686 Ma to 246 Ma. They have a variable U content of 5–393 ppm and 0.02–3.15. These ages can be grouped into two age populations of 246–573 Ma and 1,248–2,686 Ma with a main peak at ca. 261 Ma, a secondary peak at ca. 1,866 Ma, and two minor peaks at ca. 439 and 2,523 Ma (Figure 7B).

5.3 Sample D1028-1

Sixty-eight spots of 70 analyzed zircon grains yielded a concordant age of 2,785–243 Ma, with a variable U content of 12–1,244 ppm and Th/U ratio of 0.05–2.44. These spots can be grouped into three age populations of 243–469 Ma, 606–941 Ma, and 1,020–2,785 Ma. They have a main peak at ca. 254 Ma, two secondary peaks at ca. 1,908 Ma and 457 Ma, and two minor peaks at 942 Ma and 2,545 Ma (Figure 7C). These data are similar to the sample D1011-1 and D1012-1.

5.4 Sample DXT601-2

Fourteen relatively large zircons from the diabase sample DXT601-2 were analyzed, yielding concordant ages ranging from 1,470 to 210 Ma. They have a variable U content of 65–3,105 ppm and high Th/U ratio of 0.22–0.87. Four long prismatic grains of which with broad oscillatory zoning in CL images yielded Late Triassic ages between 210 and 225 Ma, with a weighted mean age of 220.0 ± 7.7 Ma (MSWD = 0.86) (Figure 7D). This age probably represents the crystalline age of the diabase.

6 Discussion

6.1 depositional age of the Maichuqing and Sanhedong Formations

Fossil data, for example *Burmesia lirata* Healey, *Cuspidaria* sp., *Prolaria sollasii* Healey, and *Nuculanna* cf. *perlonga* (Mansuy) derived from the Maichuqing Formation and *Halobia pluriradiata* Reed and *H.* cf. *yunnanensis* Reed and ammonoid, brachiopoda, and lamellibranchiate fossils in the Sanhedong Formation indicate these formations deposited during the Late Triassic (YBGMR, 1974). This is consistent with our new detrital zircon U–Pb dating results, in which the 32 youngest zircons yielded $^{206}Pb/^{238}U$ age of 243–312 Ma with the peak at ca. 254 Ma (Supplementary Table 1).

Our zircon U–Pb dating results show that the Sanhedong Formation was intruded by diabase dyke at 220.0 ± 7.7 Ma. This value provides an upper limitation for deposition time of these two formations. Accordingly, the Maichuqing and Sanhedong Formation deposited during the earliest stage (Carnian) of the Late Triassic.

6.2 possible sources of the Maichuqing and Sanhedong formations

The Maichuqing and Sanhedong formations distribute in an area that astride the Jomda–Weixi–Yuanxian arc in the west and western margin of the Yangtze Block in the east (Figure 1B). Our paleocurrent data demonstrate that the detritus of the Maichuqing Formation is mainly derived from the SW or W (215°–280°) (Figure 3). In addition, some detritus of the upper level of middle portion of this formation originated from NE-SE-ward (85°–130°) sources.

We do not consider paleocurrent data derived from the Jinding deposit (Figures 3D,E) because uncertainty in local block rotation. As such, no sedimentary data are available to constrain paleocurrent of the Sanhedong Formation. As mentioned earlier, syn-sedimentation structures (Figures 6D–F) indicates an SSW-ward slope for the related basin when the Sanhedong Formation deposited. Thus, we suggest that detritus of the Sanhedong Formation was mainly sourced from an area of NNE, where platform limestones of the Yangtze Block are common. These limestones likely have provided calcareous materials for the Sanhedong Formation.

In summary, the detritus of the Maichuqing Formation was mainly derived from the Jomda–Weixi–Yunxian arc in SSW with minor from the Yangtze Block. Detrital zircon U–Pb dating results support this suggestion. The Jomda–Weixi–Yunxian arc rocks contain many 273–248 Ma magmatic zircons as well as numerous Early Paleozoic, Late and Middle Proterozoic zircons (Figure 7E; Yang et al., 2014; Liang et al., 2015; Tang et al., 2016; Xin et al., 2018), whereas the western Yangtze Block contain voluminous Neoproterozoic and Paleoproterozic magmatic rocks (Figure 7F, e.g., Sun et al., 2009; Wang et al., 2012). On contrary, the detritus of the Sanhedong Formation probably come predominantly from the Yangtze Block in the NNE.

6.3 Tectonic evolution of Late Triassic retro-foreland basin

As mentioned earlier, the volcanic-absent Upper Triassic strata (Burchfiel and Chen, 2012) including the Maichuqing and

Sanhedong formations developed exclusively in the middle segment of the Jomda–Weixi–Yunxian arc. Structural analyses (Yang et al., 2014; Tang et al., 2016; Xin et al., 2018) have shown that Permian to Middle Triassic volcanoclastic rocks of the middle Jomda–Weixi–Yunxian arc are tightly folded. This, combined with geochemistry of volcanic rocks and granites (Xin et al., 2018) suggests that the middle segment of the Jomda–Weixi–Yunxian arc formed in responding to eastward flat subduction of Paleo-Tethys. The intensely shortened Permian to Middle Triassic volcanoclastic rocks were covered by early Late Triassic sedimentary rocks; the latter are only slightly shortened evidenced by open folds (Figure 2B). This tectonic scenario is highly comparable to the Miocene Andean retro-foreland basin in the NW Argentina (del Papa et al., 2021), where the Nazca plate flatly subducted beneath the southern American continent (e.g., Gutscher et al., 2000; Farias et al., 2008). Therefore, we infer that the basin represented by the lower Upper Triassic Maichuqing and Sanhedong Formations is a retro (arc) foreland basin corresponding the flat subduction of Paleo-Tethyan Ocean, during which the upper plate was successively shortened (Espurt et al., 2008). Meanwhile, some rocks of the basement of the upper plate were tectonically eroded as evidenced by the extremely enriched isotopic geochemistry (including zircon Lu-Hf isotopic, i.e., Yang et al., 2014; Xin et al., 2018) and the widespread inherited Yangtze-affinity zircons of the subduction-related volcanic rocks (Tang et al., 2016; Liang, 2017; Xin et al., 2018). The 220 Ma diabase dyke intruded the Sanhedong Formation probably represents the last pulse of arc-volcanism.

Available geochronological data show that, from northwest to southeast, the cessation of magmatism in the Jomda–Weixi–Yunxian arc varies from the Middle Triassic (ca. 235 Ma) to the Late Triassic (ca. 210 Ma), whereas the onset of magmatism appears to have been in the Early Permian throughout the arc (Yang et al., 2014). Different segments of the diachronous Jomda–Weixi–Yunxian arc seem to have formed due to subduction of different tectonic regimes indicated by the different type of subduction-related basins: back-arc basins developed in both the northern and southern segments (Yang et al., 2014 and references therein), whereas retro-foreland basin is solely identified in the middle segment (this study).

Paleocurrent data and syn-sedimentation structures can help to reconstruct the palaeography of the retro-foreland basins (Allen and Allen, 2005). Our paleocurrent data (Figure 3) demonstrate that a major NEE-facing slope should have been existed during deposition of the Maichuqing Formation (Figure 8A), which then shifted into a southwestward-facing one during deposition of the Sanhedong Formation (Figure 8B). We infer that, at the end of deposition of the Maichuqing Formation, the northern segment of the Paleotethyan Ocean was closed (Yang et al., 2014) and subduction along the middle segment became weak (Figure 8B). The subsequent continent-continent collision in the northern segment would have inevitably led to a higher landscape than its middle and southern equivalents whereas the oceanic subduction continued. This well explains the S- or SW-wards sliding of unsolidified sediments indicated by the syn-sedimentation structures in the upper segment of the Maichuqing Formation and in the Sanhedong Formation.

Rock assemblages and associated sedimentary structures demonstrate that the Maichuqing Formation deposited predominantly in a delta plain setting and transitional setting of the marine and terrestrial environments (Figure 8A), which evolved upward into a tide environment of costal setting for deposition of the Sanhedong Formation (Figure 8B). In addition, the thickness of the lowest part of the Maichuqing Formation rapidly increases westward (Figures 3A–C), indicating that depocenter of the retro-foreland basin should be adjacent to the west at its earliest stage (Figure 8A). On contrary, the largest accumulation of the upper segment of the Maichuqing Formation occurred in the east (Figures 3A–C). This suggest the depocenter shifted to the east immediately before the transition from the terrestrial to marine environments (Figure 8B). For other stages, the shifts of depocenter are not very clear. The depocenter shift as well as the transition in sedimentary setting probably corresponds to a significant tectonic event. The Late Triassic continental collision in the northern segment of the Jomda–Weixi–Yunxian arc (Yang et al., 2014) is an appreciate candidate.

7 Conclusion

(1) The volcanics-absent transitional unit in the SE Tibetan Plateau developed solely on the middle segment of the Jomda–Weixi–Yunxian arc owing to flat-subduction of the Paleo-Tethyan oceanic plate.
(2) The volcanics-absent transitional unit in SE Tibetan Plateau deposited within a retro-foreland basin in responds to the flat subduction during the early Late Triassic (Carnian Stage).
(3) This retro-foreland basin was filled initially by coarse-grain sediments of a delta environment, which was then gradually changed to a tidal environment of shallow marine.
(4) Syn-sedimentation structures widely developed in the retro-foreland basin, suggesting intense tectonism during sedimentation of the retro-foreland basin.

Data availability statement

The original contributions presented in the study are included in the article/Supplementary Material, further inquiries can be directed to the corresponding author.

Author contributions

TY contributed to field observations, geological-maps compiling, structural analyses, conceptualization, writing and revising, and funding acquisition. ML contributed to field observations, structural analyses, formal analyses, data processing, and draft-writing and revising. ZY contributed to field observations, draft-writing and revising. CX contributed to field observations, structural analysis, and draft-writing. DX contributed to field observations, formal analyses, and structural analysis. SQ contributed to data processing and draft-revising. PS contributed to field observations, data processing, and draft-revising. MD, WW, KX, XH and JB carried out field observations. All authors contributed to manuscript revision, read, and approved the submitted version.

Funding

This work was financially supported by the Natural Sciences Foundation of China (No. 92055206) and Ministry of Sciences and Technology of People's Republic of China (grant numbers 2016YFC0600306-4 and 2015CB452601).

Acknowledgments

This study benefited a lot from our geological mappings in SE Tibet. Numerous students have taken part in these geological mappings although the direct contribution to this study is rare. They include but not limited Cheng Liao, Lei Wang, Yunlu Yangtian, Jingkun Liu, Yuantao Yao, Lili Jiang, Liangchun Wan, Wenbin Zhu, Jing Tang, Xiaotian Li, Ruijuan Lai, and Xinpeng Yang. Dr. Zhenhui Hou helped zircon U-Pb analyses. Comments and suggestions from journal's editor and Reviewers greatly improved this manuscript.

Conflict of interest

Author PS is employed by the Beijing Jinyou Geological Exploration Co., Ltd.

The remaining authors declare that the research was conducted in the absence of any commercial or financial relationships that could be construed as a potential conflict of interest.

Publisher's note

Supplementary material

The Supplementary Material for this article can be found online at: https://www.frontiersin.org/articles/10.3389/feart.2022.957337/full#supplementary-material

References

Allen, J. R. (1982). *Sedimentary structures: Their character and physical basis, II*. Amsterdam: Elsevier.

Allen, P. A., and Allen, J. R. (2005). *Basin analysis: Principles and applications*. Oxford, UK: Wiley-Blackwell.

Alsop, G. I., and Marco, S. (2011). Soft-sediment deformation within seismogenic slumps of the dead sea basin. *J. Struct. Geol.* 33 (4), 433–457. doi:10.1016/j.jsg.2011.02.003

Anderson, T. (2002). Correction of common lead in U–Pb analyses that do not report 204Pb. *Chem. Geol.* 29, 59–79. doi:10.1016/S0009-2541(02)00195-X

Burchfiel, B. C., and Chen, Z. (2012). *Tectonics of the southeastern Tibetan plateau and its adjacent foreland*. Boulder, Colorado, USA: The Geological Society of America.

Decelles, P. G., Carrapa, B., Horton, B. K., and Gehrels, G. E. (2011). Cenozoic foreland basin system in the central Andes of northwestern Argentina: Implications for Andean geodynamics and modes of deformation. *Tectonics* 30 (TC6013). 1–30. doi:10.1029/2011TC002948

Decelles, P. G., and Giles, K. A. (1996). Foreland basin systems. *Basin Res.* 8, 105–123. doi:10.1046/j.1365-2117.1996.01491.x

del Papa, C., Payrola, P., Pingel, H., Hongn, F., Do Campo, M., Sobel, E. R., et al. (2021). Stratigraphic response to fragmentation of the Miocene Andean foreland basin, NW Argentina. *Basin Res.* 33, 2914–2937. doi:10.1111/bre.12589

Edit Committee of the Sanjiang Geological Map (1986). *1:1,000,000 geological map of the Jinshajiang, langcangjiang, nujiang regions*. Beijing: Geological Publishing House.

Espurt, N., Funiciello, F., Martinod, J., Guillaume, B., Regard, V., Faccenna, C., et al. (2008). Flat subduction dynamics and deformation of the South American plate: Insights from analog modeling. *Tectonics* 27 (TC3011). 1–19. doi:10.1029/2007TC002175

Farias, M., Charrier, R., Carretier, S., Martinod, J., Fock, A., Campbell, D., et al. (2008). Late Miocene high and rapid surface uplift and its erosional response in the Andes of central Chile (33°– 35°S). *Tectonics* 27 (TC1005). 1–22. doi:10.1029/2006TC002046

García-Castellanos, D. (2002). Interplay between lithospheric flexure and river transport in foreland basins. *Basin Res.* 14, 89–104. doi:10.1046/j.1365-2117.2002.00174.x

Griffin, W.L., Belousova, E. A., Shee, S. R., Pearson, N. J., and O'Reilly, S. Y. (2004). Archean crustal evolution in the northern Yilgarn Craton: U-Pb and Hf-isotope evidence from detrital zircons. *Precambrian Res.* 131 (3, 4), 231–282. doi:10.1016/j.precamres.2003.12.011

Gutscher, M. A., Spakman, W., Bijwaard, H., and Engdalh, E. R. (2000). Geodynamics of flat subduction: Seismicity and tomographic constraints from the Andean margin. *Tectonics* 19, 814–833. doi:10.1029/1999TC001152

Hu, X. M., Wang, J. G., BouDagher-Fadel, M., Garzanti, E., An, W., and Webb, A. (2016). The timing of India-Asia collision onset – facts, theories, controversies. *Earth-Science Rev.* 32, 264–299. doi:10.1016/j.earscirev.2016.07.014

Jordan, T. E. (1995). "Retroarc foreland and related basins," in *Tectonics of sedimentary basins*. Editors D. J. Busby and R. V. Ingersoll (Hoboken, New Jersey, United States: Blackwell Science), 331–362.

Lee, J. R., and Phillips, E. R. (2008). Progressive soft sediment deformation within a subglacial shear zone—A hybrid mosaic–pervasive deformation model for middle pleistocene glaciotectonised sediments from eastern England. *Quat. Sci. Rev.* 27 (13-14), 1350–1362. doi:10.1016/j.quascirev.2008.03.009

Li, C., Zhai, Q., Dong, Y., and Huang, X. (2006). Discovery of eclogite and its geological significance in Qiangtang area, central Tibet. *Chin. Sci. Bull.* 51, 1095–1100. doi:10.1007/s11434-006-1095-3

Liang, M. J. (2017). "Filling the Lanping basin: Response to the neotethyan tectonics in the Sanjiang orogenic belt," (Beijing, China: China University of Geosciences). Ph.D. Thesis.

Liang, M. J., Yang, T. N., Shi, P. L., Xue, C. D., Xiang, K., and Liao, C. (2015). U-Pb geochronology, Hf isotopes of zircons from the volcanic rocks along the eastern margin of Lanping basin, Sanjiang orogenic belt. *Acta Petrol. Sin.* 31 (11), 3247–3248.

Liang, M. J., Yang, T. N., Xue, C. D., Xin, D., Yan, Z., Liao, C., et al. (2022). Complete deformation history of the transition zone between oblique and orthogonal collision belts of the SE Tibetan Plateau: Crustal shortening and rotation caused by the indentation of India into Eurasia. *J. Struct. Geol.* 156, 1–18. doi:10.1016/j.jsg.2022.104545

Liao, C., Yang, T. N., Xue, C. D., Liang, M. J., Xin, D., Xiang, K., et al. (2020). Eocene basins on the SE Tibetan plateau: Markers of minor offset along the xuelongshan-diancangshan-ailaoshan structural system. *Acta Geol. Sin.* 94, 1020–1041. doi:10.1111/1755-6724.14557

Liu, X. M., Gao, S., Diwu, C. R., Yuan, H. L., and Hu, Z. C. (2007). Simultaneous *in-situ* determination of U-Pb age and trace elements in zircon by LA-ICP-MS in 20 μm spot size. *Chin. Sci. Bull.* 52, 1257–1264. doi:10.1007/s11434-007-0160-x

Lunina, O. V., Andreev, A. V., and Gladkov, A. S. (2012). The tsagan earthquake of 1862 on lake baikal revisited: A study of secondary coseismic soft-sediment deformation. *Russ. Geol. Geophys.* 53 (6), 594–610. doi:10.1016/j.rgg.2012.04.007

Miall, A. D. (1985). Architectural-element analysis: A new method of facies analysis applied to fluvial deposits. *Earth-Science Rev.* 22, 261–308. doi:10.1016/0012-8252(85)90001-7

Mo, X. X., Deng, J. F., Dong, F. L., Yu, X. H., Wang, Y., Zhou, S., et al. (2001). Volcanic petro-tectonic assemblages in the Sangjiang orogenic belt, SW China and implication for tectonics. *Geol. J. China Univ.* 7 (2), 121–138.

Moretti, M., and Sabato, L. (2007). Recognition of trigger mechanisms for soft-sediment deformation in the pleistocene lacustrine deposits of the Sant'Arcangelo basin (southern Italy): Seismic shock vs. overloading. *Sediment. Geol.* 196, 31–45. doi:10.1016/j.sedgeo.2006.05.012

Ortner, H. (2007). Styles of soft-sediment deformation on top of a growing fold system in the Gosau Group at Muttekopf, Northern Calcareous Alps, Austria: Slumping versus tectonic deformation. *Sediment. Geol.* 196 (1-4), 99–118. doi:10.1016/j.sedgeo.2006.05.028

Postma, G. (1983). Water escape structures in the context of a depositional model of a mass flow dominated conglomeratic fan-delta (Abrioja Formation, Pliocene, Almeria Basin, SE Spain). *Sedimentology* 30, 91–103. doi:10.1111/j.1365-3091.1983.tb00652.x

Reading, H. G. (1996). *Sedimentary environment: Processes, facies and stratigraphy*. 3rd Edition. Oxford: Blackwell Science.

Song, Y. C., Hou, Z. Q., Xue, C. D., and Huang, S. Q. (2020). New mapping of the world-class jinding Zn-Pb deposit, Lanping basin, southwest China: Genesis of ore host rocks and records of hydrocarbon-rock interaction. *Econ. Geol.* 115 (5), 981–1002. doi:10.5382/econgeo.4721

Steen, O., and Andresen, A. (1997). Deformational structures associated with gravitational block gliding: Examples from sedimentary olistoliths in the kalvag melange, Western Norway. *Am. J. Sci.* 297, 56–97. doi:10.2475/ajs.297.1.56

Sun, W. H., Zhou, M. F., Gao, J. F., Yang, Y. H., Zhao, X. F., and Zhao, J. H. (2009). Detrital zircon U-Pb geochronological and Lu-Hf isotopic constraints on the precambrian magmatic and crustal evolution of the Western Yangtze Block, SW China. *Precambrian Res.* 172 (1-2), 99–126. doi:10.1016/j.precamres.2009.03.010

Tang, J., Xue, C. D., Yang, T. N., Liang, M. J., Xiang, K., Liao, C., et al. (2016). Late permian to early triassic tectonostratigraphy of Madeng area, northwestern yunnan, S.W. China: Bolcanics zircon U-Pb dating. *Acta Petrol. Sin.* 32 (8), 2535–2554.

Wang, B. D., Wang, L. Q., Chen, J. L., Yin, F. G., Wang, D. B., Zhang, W. P., et al. (2014). Triassic three-stage collision in the Paleo-Tethys: Constraints from magmatism in the Jiangda–Deqen–Weixi continental margin arc, SW China. *Gondwana Res.* 26 (2), 475–491. doi:10.1016/j.gr.2013.07.023

Wang, B. D., Wang, L. Q., Qiangba, Z. X., Zeng, Q. G., Zhang, W. P., Wang, D. B., et al. (2011). Early Triassic collision of Northern Lancangjiang suture: Geochronological, geochemical and Hf isotope evidence from the granitic gneiss in Leiwuqi area, eastern Tibet. *Acta Petrol. Sin.* 27, 2752–2762.

Wang, L. J., Yu, J. H., Griffin, W. L., and O'Reilly, S. Y. (2012). Early crustal evolution in the Western Yangtze Block: Evidence from U–Pb and Lu–Hf isotopes on detrital zircons from sedimentary rocks. *Precambrian Res.* 222-223, 368–385. doi:10.1016/j.precamres.2011.08.001

Wiedenbeck, M., Allé, P., Corfu, F., Griffin, W. L., Meier, M., Oberli, F., et al. (1995). Three natural zircon standards for U-Th-Pb, Lu-Hf, trace element and REE analyses. *Geostand. Geoanal. Res.* 19, 1–23. doi:10.1111/j.1751-908X.1995.tb00147.x

Xin, D., Yang, T. N., Liang, M. J., Xue, C. D., Han, X., Liao, C., et al. (2018). Synsubduction crustal shortening produced a magmatic flare-up in middle Sanjiang orogenic belt, southeastern Tibet plateau: Evidence from geochronology, geochemistry, and structural geology. *Gondwana Res.* 62, 93–111. doi:10.1016/j.gr.2018.03.009

Yang, T. N., Ding, Y., Zhang, H. R., Fan, J. W., Liang, M. J., and Wang, X. H. (2014). Two-phase subduction and subsequent collision defines the paleotethyan tectonics of the southeastern Tibetan plateau: Evidence from zircon U-Pb dating, geochemistry, and structural geology of the Sanjiang orogenic belt, southwest China. *Geol. Soc. Am. Bull.* 126, 1654–1682. doi:10.1130/B30921.1

Yang, T. N., Hou, Z. Q., Wang, Y., Zhang, H. R., and Wang, Z. L. (2012). Late paleozoic to early mesozoic tectonic evolution of northeast Tibet: Evidence from the triassic composite Western jinsha-garze-litang suture. *Tectonics* 31 (TC4004). 1–20. doi:10.1029/2011TC003044

Yang, T. N., Yan, Z., Xue, C. D., Xin, D., and Dong, M. M. (2021). India indenting eurasia: A brief review and new data from the yongping basin on the SE Tibetan plateau. *Geosciences* 11, 1–29. doi:10.3390/geosciences11120518

Yang, T. N., Zhang, H. R., Liu, Y. X., Wang, Z. L., Song, Y. C., Yang, Z. S., et al. (2011). Permo-Triassic arc magmatism in central Tibet: Evidence from zircon U–Pb geochronology, Hf isotopes, rare Earth elements, and bulk geochemistry. *Chem. Geol.* 284, 270–282. doi:10.1016/j.chemgeo.2011.03.006

YBGMR (Yunnan Bureau of Geology and Mineral Resource) (1974). *Geological map (scale 1/200,000) with geological report of Lanping (block G-47-X VI)*. Kunming, Yunnan: Yunnan Bureau of Geology and Mineral Resource.

Yuan, H. L., Gao, S., Liu, X. M., Li, H. M., Gunther, D., and Wu, F. Y. (2004). Accurate U–Pb age and trace element determinations of zircon by laser ablation-inductively coupled plasma-mass spectrometry. *Geostand. Geoanal. Res.* 28, 353–370. doi:10.1111/j.1751-908x.2004.tb00755.x